LPT 96–15
TK 96 21

arXiv:hep-ph/9607428v1 25 Jul 1996

NUCLEON ELECTROWEAK FORM FACTORS: ANALYSIS OF THEIR SPECTRAL FUNCTIONS

V. Bernard[‡], N. Kaiser[◇], Ulf-G. Meißner[†#1]

[‡]Université Louis Pasteur, Laboratoire de Physique Théorique
BP 28, F–67037 Strasbourg, France
email: bernard@crnhp4.in2p3.fr

[◇]Technische Universität München, Physik Department T39
James-Franck-Straße, D–85747 Garching, Germany
email: : nkaiser@physik.tu-muenchen.de

[†]Universität Bonn, Institut für Theoretische Kernphysik
Nussallee 14-16, D–53115 Bonn, Germany
email: meissner@itkp.uni-bonn.de

Abstract

We investigate the imaginary parts of the nucleon electromagnetic and axial form factors close to threshold in the framework of heavy baryon chiral perturbation theory. For the isovector electromagnetic form factors, we recover the well known strong enhancement near threshold. For the isoscalar ones, we show that there is no visible enhancement due to the three–pion continuum. This justifies the use of vector meson poles only in dispersion–theoretical calculations. We also calculate the imaginary part of the nucleon isovector axial form factor and show that it is small in the threshold region.

[#1]Address after Oct. 1, 1996: FZ Jülich, IKP (Theorie), D-52425 Jülich, Germany

I. INTRODUCTION AND SUMMARY

The electromagnetic and axial structure of the nucleon as revealed e.g. in elastic electron–nucleon and (anti)neutrino–nucleon scattering is parameterized in terms of the six form factors $F_{1,2}^{p,n}(t)$ and $G_{A,P}(t)$[#2] (with t the squared momentum transfer). The understanding of these form factors is of utmost importance in any theory or model of the strong interactions. Abundant data on these form factors over a large range of momentum transfer exist and this data base will increase when the recent/upcoming experiments performed at ELSA, MAMI and TJNAL will have been analyzed. Dispersion theory is a tool to interpret (and cross check) these data in a largely model–independent fashion. The form factors can be written in terms of unsubtracted dispersion relations and their absorptive parts are often parameterized in terms of a few vector meson poles. This procedure is based on the successful vector meson dominance (VMD) hypothesis, which states that a photon (or W/Z–boson) couples to hadrons only via intermediate vector mesons. However, as already pointed out in 1959 by Frazer and Fulco [1], such an approach is not in conformity with general constraints from unitarity and analyticity. In particular the singularity structure of the triangle diagram is not respected at all when using only vector meson poles. As a consequence of this singularity structure the two–pion continuum has a pronounced effect on the isovector spectral functions on the left wing of the ρ–resonance. This becomes particularly visible in the determinations of the corresponding nucleon mean square radii. This effect was quantified by the Karlsruhe–Helsinki group in their seminal work on the nucleon electromagnetic form factors [2,3]. This analysis was recently refined by the Mainz–Bonn group accounting for new data and the high energy constraints from perturbative QCD [4,5]. However, there still remains one open end concerning the dispersion–theoretical analysis. In the isoscalar electromagnetic channel, it is believed (but not proven) that the pertinent spectral functions rise smoothly from the three–pion threshold to the ω-meson peak, i.e. that there is no pronounced effect from the three–pion cut on the left wing of the ω-resonance (which also has a much smaller width than the ρ-meson). Chiral perturbation theory [6,7] can be used to settle this issue. An investigation of the isoscalar spectral functions based on pion scattering data and dispersion theory as done for the isovector spectral functions [2,3] seems not to be feasible at the moment since it requires the full dispersion–theoretical analysis of the three-body processes $\pi N \to \pi\pi N$ (or of the data on $\bar{N}N \to 3\pi$).

The one loop calculation of the isovector nucleon form factors indeed shows the strong unitarity correction on the left wing of the ρ-meson (i.e. slightly above threshold) [6,7]. For the isoscalar form factors, a calculation of the imaginary parts of certain two–loop diagrams will reveal whether there is some enhancement above $t = 9M_\pi^2$ or justify the common assumption that one has a smooth isoscalar spectral functions driven by the ω-meson at low t. Similarly, the spectral function of the isovector axial form factor is supposedly dominated by correlated $\pi\rho$-exchange (or the a_1-meson) in the region above threshold. Nothing is yet known about a possible strong enhancement of the pertinent imaginary part slightly above threshold. It is exactly this problem we wish to address in this paper by evaluating the imaginary parts of the pertinent two loop diagrams at chiral order q^7 and q^5 contributing to the isoscalar electromagnetic and the isovector axial form factors in the framework of heavy baryon chiral perturbation theory.

[#2] In what follows, we will not be concerned with the induced pseudoscalar form factor $G_P(t)$ which is dominated by its pion–pole term $4g_{\pi N}mF_\pi/(M_\pi^2 - t)$.

The pertinent results of this investigation can be summarized as follows:

(i) We have calculated the imaginary parts of the isovector electromagnetic form factors in heavy baryon CHPT to order q^4 (in the effective Lagrangian), thus extending previous studies [6,7]. The strong enhancement slightly above threshold on the left wing of the ρ-resonance due to the two–pion continuum is recovered and good agreement with the empirical analysis is found if one subtracts from it the ρ–meson contribution (by setting the pion charge form factor $F_\pi^V(t) \equiv 1$) as described in section III).

(ii) We have determined the leading contribution to the imaginary parts of the isoscalar electromagnetic form factors in the threshold region by evaluating the imaginary part of the relevant two–loop diagrams at order q^7. As previously anticipated, these imaginary parts are very small and rise smoothly with increasing t. The common procedure [3] [4] of describing the isoscalar electromagnetic spectral functions by the ω-meson pole (and higher mass poles and/or continua) is therefore justified.

(iii) We have also calculated the imaginary part of the nucleon isovector axial form factor in the threshold region. It shows a behavior similar to the isoscalar electromagnetic spectral functions, i.e. a smooth rise from threshold. Furthermore, this three–pion contribution is numerically small.

II. BASIC CONCEPTS

In this section, we assemble all necessary definitions for the calculation of the imaginary parts (spectral distributions) discussed below. This section serves mainly the purpose of fixing the notation underlying our analysis. This material is mostly not new but necessary to keep the manuscript self–contained. The reader familiar with it is invited to skip this section.

Consider first the nucleon electromagnetic form factors. They are defined by the nucleon matrix element of the quark electromagnetic current,

$$\langle N(p')|\bar{q}\gamma^\mu Q q|N(p)\rangle = \bar{u}(p')\Big[\gamma^\mu\, F_1(t) + \frac{i}{2m}\sigma^{\mu\nu}(p'-p)_\nu\, F_2(t)\Big]u(p) \tag{1}$$

with $t = (p'-p)^2$ the invariant momentum transfer squared and Q the quark charge matrix, $Q = \mathrm{diag}(\frac{2}{3}, -\frac{1}{3}, -\frac{1}{3})$. $F_1(t)$ and $F_2(t)$ are called the Dirac and Pauli form factors, in order. Following the conventions of [4], the electromagnetic form factors are decomposed into isoscalar (S) and isovector (V) components

$$F_{1,2}(t) = F_{1,2}^S(t) + \tau^3 F_{1,2}^V(t) \quad , \tag{2}$$

subject to the normalization

$$F_1^S(0) = F_1^V(0) = \frac{1}{2}\,, \quad F_2^S(0) = \frac{\kappa_p+\kappa_n}{2}\,, \quad F_2^V(0) = \frac{\kappa_p-\kappa_n}{2} \ , \tag{3}$$

with $\kappa_p = 1.793$ ($\kappa_n = -1.913$) the anomalous magnetic moment of the proton (neutron). In what follows, we will work with the electric and magnetic (Sachs) form factors,

$$G_E^{S,V}(t) = F_1^{S,V}(t) + \frac{t}{4m^2} F_2^{S,V}(t)\,, \quad G_M^{S,V}(t) = F_1^{S,V}(t) + F_2^{S,V}(t) \tag{4}$$

in the isospin basis, and $m = 938.27$ MeV denotes the nucleon mass.

Similarly, the nucleon matrix element of the quark isovector axial current is parameterized in terms of two form factors,

$$\langle N(p')|\bar{q}\gamma^\mu\gamma_5\tau^a q|N(p)\rangle = \bar{u}(p')\Big[\gamma^\mu\, G_A(t) + \frac{1}{2m}(p'-p)^\mu\, G_P(t)\Big]\gamma_5\tau^a u(p)\ , \tag{5}$$

with $G_A(t)$ called the axial and $G_P(t)$ the induced pseudoscalar form factor. In what follows, we will only be concerned with the axial form factor. Its normalization is given by $G_A(0) = g_A = 1.26$.

We briefly discuss now the pertinent dispersion relations. Let $F(t)$ be a generic symbol for any one of the five nucleon electroweak form factors. We assume the validity of an unsubtracted dispersion relation of the form

$$F(t) = \frac{1}{\pi}\int_{t_0}^{\infty} \frac{\mathrm{Im}\, F(t')}{t'-t-i\epsilon}\, dt'\ , \tag{6}$$

where the $-i\epsilon$ in the numerator is necessary if $t > t_0$, since in that region $F(t)$ is complex valued. The spectral function Im $F(t)$ is different from zero along the cut from t_0 to $+\infty$ on the real t-axis, with $t_0 = 9\,M_\pi^2$ for the isoscalar electromagnetic and the axial case. $M_\pi = 139.57$ MeV denotes the pion mass and we neglect isospin breaking effects in the pion and nucleon masses. For the isovector electromagnetic form factors the threshold lies at $t_0 = 4\,M_\pi^2$. The proof of the validity of such dispersion relations in QCD has not yet been given [8]. Eq.(6) means that the electroweak structure of the nucleon is entirely determined from its absorptive behavior, with the data for $F(t)$ given (mainly) for $t \leq 0$. In what follows, we will concentrate on the threshold behavior of the various spectral functions, i.e. the range $t_0 \leq t \leq 30\,M_\pi^2$. The upper end of this range corresponds to the mass of the first isoscalar and isovector vector mesons, i.e. the ω- and the ρ-meson ($M_\omega^2 = 31.4\,M_\pi^2$, $M_\rho^2 = 30.3\,M_\pi^2$).

III. ISOVECTOR ELECTROMAGNETIC SPECTRAL FUNCTIONS

Unitarity determines the spectral functions of the isovector electromagnetic form factors in the interval $4M_\pi^2 < t < 16M_\pi^2$ uniquely as,[#3]

$$\begin{aligned}
\mathrm{Im}\, G_E^V(t) &= \frac{(t-4M_\pi^2)^{3/2}}{8m\sqrt{t}}\, f_+^1(t)\, F_\pi^{V\,*}(t)\,, \\
\mathrm{Im}\, G_M^V(t) &= \frac{(t-4M_\pi^2)^{3/2}}{8\sqrt{2t}}\, f_-^1(t)\, F_\pi^{V\,*}(t)\ ,
\end{aligned} \tag{7}$$

with $F_\pi^V(t)$ the pion charge form factor and the $f_\pm^1(t)$ are the P–wave πN partial wave amplitudes in the t–channel ($\pi\pi \to \bar{N}N$), cf. fig. 1. The partial wave amplitudes $f_\pm^1(t)$ have

[#3] In practise, this representation holds up to $t \simeq 50\,M_\pi^2$.

a logarithmic singularity on the second Riemann sheet [3] (originating from the projection of the nucleon pole terms in the invariant πN scattering amplitudes) located at

$$t_c = 4M_\pi^2 - M_\pi^4/m^2 = 3.98\, M_\pi^2 \ , \tag{8}$$

very close to the physical threshold at $t_0 = 4M_\pi^2$. The isovector form factors inherit this singularity (on the second sheet) and the closeness to the physical threshold leads to the pronounced enhancement of the isovector spectral functions weighted with $1/t^2$ as shown in fig. 2. Note that the ratio of the magnetic to the electric spectral function is very close to $1 + \kappa_p - \kappa_n = 4.71$, i.e. the ratio of the form factors in dipole approximation. For later comparison, we also show the corresponding curves with $F_\pi^V(t) \equiv 1$ (to suppress the contribution from the ρ–meson). This strong enhancement is obviously very important for a precise determination of the nucleon isovector mean square radii [2,4].

In the framework of relativistic baryon CHPT, the isovector spectral functions were calculated in [6]. The correct analytic structure naturally emerged in this calculation and thus the strong threshold enhancement. However, in that framework there is no consistent power counting scheme due to the extra energy scale related to the nucleon mass in the chiral limit. This can be overcome in the heavy baryon approach, which is discussed in detail in the review [7]. In that paper, the imaginary parts of the isovector Dirac and Pauli form factors were calculated to order q^3 and compared to the result of [6]. Here, we go one step further and calculate also the first corrections to these results at order q^4, thus completing the one loop calculation. The imaginary part of the isovector electric form factor can be given entirely in terms of lowest order parameters

$$\mathrm{Im}\, G_E^V(t) = \frac{\sqrt{t-4M_\pi^2}}{192\pi F_\pi^2 \sqrt{t}}\Big[t - 4M_\pi^2 + g_A^2(5t - 8M_\pi^2)\Big] - \frac{g_A^2 (t-2M_\pi^2)^2}{128 m F_\pi^2 \sqrt{t}} \ , \tag{9}$$

where the term in the square brackets is the order q^3 result and $F_\pi = 92.4$ MeV is the pion decay constant. We remark that in the expressions for the imaginary parts we make use of the Goldberger-Treiman relation to determine the value of g_A, $g_A = g_{\pi N} F_\pi/m = 1.32$, since here the pion-nucleon coupling constant $g_{\pi N} = 13.4$ appears naturally and not the axial current coupling g_A. The expression for the imaginary part of the isovector magnetic form factor to order q^4 contains the low–energy constant c_4 of the dimension two pion–nucleon Lagrangian (we take the value $c_4 = 2.25\,\mathrm{GeV}^{-1}$ determined in [9] from some πN data),

$$\mathrm{Im}\, G_M^V(t) = \frac{g_A^2 m (t-4M_\pi^2)}{64 F_\pi^2 \sqrt{t}} + \frac{\sqrt{t-4M_\pi^2}}{192\pi F_\pi^2 \sqrt{t}}\Big[(1+4mc_4)(t-4M_\pi^2) + g_A^2(16M_\pi^2 - 7t)\Big] \ . \tag{10}$$

We remark that at this order the normal threshold $t_0 = 4M_\pi^2$ and the anomalous threshold $t_c = 4M_\pi^2 - M_\pi^4/m^2$ on the second Riemann sheet still coalesce (it requires accuracy q^5 to separate t_0 and t_c). As a consequence of this, the isovector imaginary parts show an abnormal threshold behavior in the $1/m$ expansion, i.e. they do not start out as $(t-4M_\pi^2)^{3/2}$ as in eq.(7). The coalescence of both thresholds leads to smaller exponents. This problem is, however, largely academic as the comparison of the so calculated imaginary parts (weighted with $1/t^2$) shown in fig. 3 with the dashed–dotted lines of fig. 2 reveals (one should only compare to the empirical spectral functions with the contribution of the ρ-meson subtracted since this resonance is not included in the effective field theory). In fig. 3, the results of the order q^3 and order q^4 calculations are shown separately by the dashed and solid lines, respectively, indicating that the empirical observation of the strong peak close to threshold can indeed be explained within the heavy mass expansion of the chiral effective pion–nucleon field theory. This shows that the method can be used to investigate the isoscalar spectral distributions in the threshold region (below the ω-resonance).

IV. ISOSCALAR ELECTROMAGNETIC SPECTRAL FUNCTIONS

The imaginary parts of the isoscalar electromagnetic form factors open at the three–pion threshold $t_0 = 9\,M_\pi^2$. The three–pion cut contribution is depicted in fig. 4. In the $\bar{N}N$ center-of-mass system, the pertinent anti-nucleon and nucleon four–momenta are $p_1^\mu = (\sqrt{t}/2, \vec{p})$ and $p_2^\mu = (\sqrt{t}/2, -\vec{p})$. The analytic continuation of the three–momentum $\vec{p}$ into the region $t < 4\,m^2$ takes the form

$$\vec{p} = \hat{p}\,\sqrt{t/4 - m^2} = i\,m\,\hat{p} + \ldots \ . \tag{11}$$

in the heavy mass expansion, with $\hat{p}$ a real unit vector. Application of the Cutkosky rules to three–pion intermediate state with four–momenta l_1, l_2 and $l_3 = p_1 + p_2 - l_1 - l_2$ (cf. fig. 4) leads to

$$\mathrm{Im}\left[A \int \frac{d^4 l_1}{i(2\pi)^4} \int \frac{d^4 l_2}{i(2\pi)^4} \frac{1}{M_\pi^2 - l_1^2} \frac{1}{M_\pi^2 - l_2^2} \frac{1}{M_\pi^2 - l_3^2}\, B\right] = \frac{1}{2} \int d\Gamma_3 (A\,B) \ , \tag{12}$$

where the symbol 'A' refers to the $\gamma \to 3\pi$ and 'B' to the $3\pi \to \bar{N}N$ transition, respectively, and $d\Gamma_3$ is the measure on the invariant three–body phase space. In what follows, we have to evaluate integrals over the three–pion phase space. Tensorial integrals can be reduced to scalar ones by the following formula (or any permutation of it in the indices '1' and '2')

$$\begin{aligned} \int d\Gamma_3\, H(\ldots)\, \hat{l}_1^i\, \hat{l}_1^j\, \hat{l}_2^k = \int d\Gamma_3\, H(\ldots) \Big[& \frac{y}{2}(1-x^2)\delta^{ij}\,\hat{p}^k + \frac{x}{2}(z - xy)(\delta^{ik}\,\hat{p}^j + \delta^{jk}\,\hat{p}^i\,) \\ & + (\frac{y}{2}(5x^2 - 1) - xz)\,\hat{p}^i\,\hat{p}^j\,\hat{p}^k \Big] \end{aligned} \tag{13}$$

with

$$\begin{aligned} & |\vec{l}_i| = \sqrt{\omega_i^2 - M_\pi^2}\ , \ (i = 1, 2)\ , \quad x = \hat{l}_1 \cdot \hat{p}\ , \quad y = \hat{l}_2 \cdot \hat{p}\ , \\ & z = \hat{l}_1 \cdot \hat{l}_2 = \frac{\omega_1\omega_2 - \sqrt{t}(\omega_1 + \omega_2) + \frac{1}{2}(t + M_\pi^2)}{|\vec{l}_1|\,|\vec{l}_2|} \quad , \end{aligned} \tag{14}$$

and the function $H(\ldots)$ depends on the variables $\omega_1, \omega_2, x, y, z, t$. The integration over the three-pion phase space can be expressed as a four-dimensional integral of the form

$$\frac{1}{2} \int d\Gamma_3\, H(\ldots) = \frac{1}{128\pi^4} \int \int_{z^2<1} d\omega_1 d\omega_2 \int \int_E \frac{dx dy}{\sqrt{1 - x^2 - y^2 - z^2 + 2xyz}}\, H(\ldots) \ , \tag{15}$$

where the interior of the ellipse E is defined by the equation $1 - x^2 - y^2 - z^2 + 2xyz > 0$. The ellipse has semi–axes of length $\sqrt{1-z}$ and $\sqrt{1+z}$, respectively.

In chiral perturbation theory, to leading order q^7, the two–loop diagrams shown in fig. 5 can contribute to the isoscalar imaginary parts, but graph (d) vanishes because of an isospin factor zero. All (relativistic) Feynman rules needed to calculate these graphs can be recovered from appendix A of [7] with the exception of the anomalous $\gamma 3\pi$ vertex. In the chiral effective Lagrangian approach, it follows from the Wess–Zumino–Witten term (for a review, see [10]),

$$\mathcal{L}^{(4)}_{\pi\pi} = \frac{e\,\epsilon^{\mu\nu\alpha\beta}}{48\pi^2}\,A_\mu\,\mathrm{Tr}\,(\partial_\nu U U^\dagger\,\partial_\alpha U U^\dagger\,\partial_\beta U U^\dagger\,)\ , \tag{16}$$

with A_μ the photon field and $U = 1 + i\vec{\tau}\cdot\vec{\pi}/F + \ldots$ collects the pions. Note that this vertex has dimension four and therefore the two–loop graphs for the imaginary parts start only at order q^7. The corresponding Feynman insertion (with the sign convention $\epsilon^{0123} = -1$) is

$$\gamma 3\pi - \text{vertex}: \quad -\frac{e\,\sqrt{t}}{4\pi^2 F_\pi^3}\,\vec{\epsilon}\cdot(\vec{l}_1\times\vec{l}_2\,)\,\epsilon^{abc} \tag{17}$$

where $'a,b,c'$ are pion isospin indices and $\vec{\epsilon}$ is the photon polarization vector. With these rules at hand and using eqs.(11–15) one arrives after straightforward but tedious calculations at the isoscalar imaginary parts in the limit $m\to\infty$. We give only the results in this limit since these represent the genuine leading order contributions with all higher order effects (starting at order q^8) switched off. Furthermore, only in this limit the angular integrations in eq.(15) can be performed analytically. We find:

$$\mathrm{Im}\,G_E^S(t) = \frac{3g_A^3\,t}{(4\pi)^5 F_\pi^6}\int\!\!\int_{z^2<1} d\omega_1 d\omega_2\,|\vec{l}_1|\,|\vec{l}_2|\,\sqrt{1-z^2}\,\arccos(-z)\ , \tag{18}$$

$$\begin{aligned}\mathrm{Im}\,G_M^S(t) = \frac{g_A m}{(8\pi)^4 F_\pi^6}\Big\{&L(t)\Big[3t^2 - 10tM_\pi^2 + 2M_\pi^4 + g_A^2(3t^2 - 2tM_\pi^2 - 2M_\pi^4)\Big]\\ &+W(t)\Big[t^3 + 2t^{5/2}M_\pi - 39t^2M_\pi^2 - 12t^{3/2}M_\pi^3 + 65tM_\pi^4 - 50\sqrt{t}M_\pi^5 - 27M_\pi^6\\ &+g_A^2(5t^3 + 10t^{5/2}M_\pi - 147t^2M_\pi^2 + 36t^{3/2}M_\pi^3 + 277tM_\pi^4 - 58\sqrt{t}M_\pi^5 - 135M_\pi^6)\Big]\Big\}\ ,\end{aligned} \tag{19}$$

with

$$L(t) = \frac{M_\pi^4}{2t^{3/2}}\ln\frac{\sqrt{t} - M_\pi + \sqrt{t - 2\sqrt{t}M_\pi - 3M_\pi^2}}{2M_\pi}\ , \tag{20}$$

$$W(t) = \frac{\sqrt{t} - M_\pi}{96t^{3/2}}\sqrt{t - 2\sqrt{t}M_\pi - 3M_\pi^2}\ . \tag{21}$$

Note that in the infinite nucleon mass limit $\mathrm{Im}\,G_E^S(t)$ comes solely from graph (c) in fig. 5 and quite astonishingly one can evaluate all integrals in closed form for $\mathrm{Im}\,G_M^S(t)$. For the sake of completeness we give also the isoscalar electromagnetic spectral functions in the chiral limit $M_\pi = 0$. The resulting expressions can be given in closed form,

$$\mathrm{Im}\ \mathring{G}_E^S\,(t) = \frac{1}{105}\Big(\frac{\mathring{g}_A\ t}{16\pi F^2}\Big)^3\ , \qquad \mathrm{Im}\ \mathring{G}_M^S\,(t) = \frac{\mathring{g}_A\,(1+5\,\mathring{g}_A^2)\,\mathring{m}\ t^{5/2}}{6(16\pi)^4 F^6}\ , \tag{22}$$

and exhibit a simple power like dependence on the variable t. In eq.(22) all quantities are to be taken at their values in the chiral limit, as denoted by the '$\circ$', with the exception of the pion decay constant whose chiral limit value is called F. The behavior near threshold $t_0 = 9\,M_\pi^2$ of the imaginary parts for finite pion mass, eqs.(18,19), is

$$\mathrm{Im}\, G_E^S(t) \sim (\sqrt{t} - 3M_\pi)^3\,, \qquad \mathrm{Im}\, G_M^S(t) \sim (\sqrt{t} - 3M_\pi)^{5/2} \tag{23}$$

which corresponds to a stronger growth than pure phase space

$$\int\!\!\int_{z^2<1} d\omega_1 d\omega_2\, |\vec{l}_1 \times \vec{l}_2|^2 \sim (\sqrt{t} - 3M_\pi)^4 \ . \tag{24}$$

This feature indicates (as in the isovector case) that in the heavy nucleon mass limit $m \to \infty$ normal and anomalous thresholds coincide. In order to find these singularities for finite nucleon mass m an investigation of Landau equations is necessary [11]. By using standard techniques [11] we are able find (at least) one anomalous threshold of diagrams (a) and (b) at

$$\sqrt{t_c} = M_\pi\left(\sqrt{4 - M_\pi^2/m^2} + \sqrt{1 - M_\pi^2/m^2}\right)\,, \qquad t_c = 8.90\, M_\pi^2 \tag{25}$$

which is very near to the (normal) threshold $t_0 = 9\, M_\pi^2$ and indeed coalesces with t_0 in the infinite nucleon mass limit. We note that diagram (d) does not possess this anomalous threshold $t_c = 8.90\, M_\pi^2$, but only the normal one. We do not want to go here deeper into the rather complicated analysis of the full singularity structure of all two-loop diagrams in fig. 5 but are mainly interested in the magnitude of the isoscalar electromagnetic imaginary parts. The resulting spectral distributions again weighted with $1/t^2$ are shown in fig. 6. They show a smooth rise and are two orders of magnitude smaller than the corresponding isovector ones, cf. fig. 3. This smallness justifies the procedure in the dispersion–theoretical analysis like in [4] to describe the isoscalar spectral functions solely by vector meson poles starting with the ω-meson in the low energy region. Nevertheless, it may be worthwhile to include these calculated isoscalar imaginary parts in future dispersion analyses. We finally remark, that $\mathrm{Im}\ G_{E,M}^S(t)/t^4$ which have the same asymptotic behavior (for $t \to \infty$) as $\mathrm{Im}\ G_{E,M}^V(t)/t^2$ (considering only the leading q^3 contribution) do still not show any strong peak below the ω–resonance. $\mathrm{Im}\ G_E^S(t)/t^4$ is monotonically increasing from $t_0 = 9\, M_\pi^2$ to $t = 30\, M_\pi^2$ and $\mathrm{Im}\ G_M^S(t)/t^4$ develops some plateau between $t = 20$ and $30\, M_\pi^2$. This observation is a further indication that there is indeed no enhancement of the isoscalar electromagnetic spectral function near threshold. Even though the isoscalar and isovector electromagnetic form factors behave formally very similar concerning the existence of anomalous thresholds t_c very close to the normal thresholds t_0, the influence of these on the physical spectral functions is rather different for the two cases. Only in the isovector case a strong enhancement is visible. This is presumably due to the different phase space factors, which are $(t - t_0)^{3/2}$ and $(t - t_0)^4$ for the isovector and isoscalar case, respectively. In latter case, the anomalous threshold at $t_c = 8.9\, M_\pi^2$ is thus effectively masked.

V. ISOVECTOR AXIAL SPECTRAL FUNCTION

The calculation of the imaginary part of the axial form factor $\mathrm{Im}\ G_A(t)$ proceeds along the same lines as outlined in the previous section. One has to consider the same graphs shown in fig. 5 (with the wiggly line denoting now the external axial source, i.e. the W–boson). All four graphs contribute and performing the necessary integrations, the imaginary part of $G_A(t)$ in the heavy mass limit reads

$$\mathrm{Im}\, G_A(t) = \frac{g_A}{192\pi^3 F_\pi^4} \int\int_{z^2<1} d\omega_1 d\omega_2 \Big\{ 6g_A^2(\sqrt{t}\,\omega_1 - M_\pi^2)\Big(\frac{|\vec{l}_2|}{|\vec{l}_1|} + z\Big)\frac{\arccos(-z)}{\sqrt{1-z^2}} \\ +2g_A^2(M_\pi^2 - \sqrt{t}\,\omega_1 - \omega_1^2) + M_\pi^2 - \sqrt{t}\,\omega_1 + 2\omega_1^2 \Big\}\ . \qquad (26)$$

In the chiral limit $M_\pi = 0$ the isovector axial spectral function shows a simple t^2 dependence of the form

$$\mathrm{Im}\ \overset{\circ}{G}_A\,(t) = \frac{\overset{\circ}{g}_A\ t^2}{(16\pi)^3 F^4}\Big[\overset{\circ}{g}{}_A^2\,\Big(K - \frac{22}{9}\Big) - \frac{2}{9}\Big]\ , \qquad K = 6.663\ . \qquad (27)$$

We remark again that the behavior near threshold,

$$\mathrm{Im}\, G_A(t) \sim (\sqrt{t} - 3M_\pi)^2 \qquad (28)$$

is a stronger rise than pure phase space

$$\int\int_{z^2<1} d\omega_1 d\omega_2\, |\vec{l}_1|\, |\vec{l}_2| \sim (\sqrt{t} - 3M_\pi)^3\ \ . \qquad (29)$$

If one considers individual diagrams one finds that only the graphs (a), (b) and (c) which have intermediate nucleon propagators show the stronger threshold behavior of eq.(28). Diagram (d) without a nucleon propagator follows the phase space argument eq.(29). The obvious reason for these features is the coincidence of normal and anomalous threshold in graphs (a), (b) and (c) which does not occur in diagram (d) in the limit $m \to \infty$ Finally, fig. 7 shows the isovector axial spectral function $\mathrm{Im}\, G_A(t)$ which again has a smooth rise from threshold and is about one order of magnitude smaller than the isovector electric spectral function. Even though $\mathrm{Im}\, G_A(t)$ starts at order q^5 it is only three times as large as the isoscalar magnetic spectral function $\mathrm{Im}\, G_M^S(t)$ of order q^7. We remark that Im $G_A(t)/t^3$, which has the same asymptotics as Im $G_E^V(t)/t^2$ (to order q^3), is still monotonically increasing from threshold to $t = 30\, M_\pi^2$, indicating once more that the three-pion continuum has no pronounced effect on the axial spectral function near threshold. Of course, one also has to keep in mind that the available data for $G_A(t)$ are not yet that precise to perform accurate dispersion–theoretical calculation.

This completes our analysis of the spectral functions related to the isoscalar electromagnetic and isovector axial nucleon form factors near threshold. We do not find a visible strong enhancement slightly above threshold $t_0 = 9\, M_\pi^2$ as in the isovector electromagnetic case, even though these imaginary parts do not follow the phase space in the heavy nucleon mass limit. The presence of a nearby anomalous threshold at $t_c = 8.9\, M_\pi^2$ has no substantial effect on the strength of the three–pion continuum.

REFERENCES

[1] W.R. Frazer and J.R. Fulco, *Phys. Rev. Lett.* **2** (1959) 365; *Phys. Rev.* **117** (1960) 1603, 1609.

[2] G. Höhler and E. Pietarinen, *Phys. Lett.* **B53** (1975) 471.

[3] G. Höhler et al., *Nucl. Phys.* **B114** (1976) 505; G. Höhler, in Landolt-Börnstein, Vol. 9b2, ed H. Schopper (Springer, Berlin, 1983).

[4] P. Mergell, Ulf–G. Meißner and D. Drechsel, *Nucl. Phys.* **A597** (1995) 367.

[5] H.–W. Hammer, Ulf–G. Meißner and D. Drechsel, *Phys. Lett.* **B367** (1996) 323; *Phys. Lett.* **B** (1996) in print [hep-ph/9604294].

[6] J. Gasser, M.E. Sainio and A. Švarc, *Nucl. Phys.* **B307** (1988) 779.

[7] V. Bernard, N. Kaiser and Ulf-G. Meißner, *Int. J. Mod. Phys.* **E4** (1995) 193.

[8] R. Oehme, πN Newsletter **7** (1992) 1.

[9] V. Bernard, N. Kaiser and Ulf-G. Meißner, *Nucl. Phys.* **B457** (1995) 147.

[10] J. Bijnens, *Int. J. Mod. Phys.* **A8** (1993) 3045.

[11] R.J. Eden, P.V. Landshoff, D.I. Olive and J.C. Polkinghorne, *The Analytic S–Matrix* (Cambridge University Press, Cambridge, 1966).

Figure captions

Fig.1 Two–pion cut contribution to the nucleon isovector electromagnetic form factors. Wiggly, dashed and solid lines represent photons, pions and nucleons, in order.

Fig.2 Spectral distribution of the isovector electric and magnetic nucleon form factors weighted with $1/t^2$ on the left wing of the ρ–resonance as calculated in [4]. Shown are $\mathrm{Im}\, G_M^V(t)/t^2$ (upper solid line) and $\mathrm{Im}\, G_E^V(t)/t^2$ (lower solid line). Suppressing the ρ–meson contribution as described in the text ($F_\pi^V(t) \equiv 1$) leads to the respective dashed–dotted lines.

Fig.3 Spectral distribution of the isovector electric and magnetic nucleon form factors weighted with $1/t^2$ calculated in heavy baryon CHPT. Shown are $\mathrm{Im}\, G_M^V(t)/t^2$ (upper lines) and $\mathrm{Im}\, G_E^V(t)/t^2$ (lower lines). The solid and dashed lines refer to the order q^4 and q^3 calculations, respectively.

Fig.4 Three–pion cut contribution to the nucleon isoscalar electromagnetic form factors. The vertex denoted 'A' describes the $\gamma \to 3\pi$ coupling and the one denoted 'B' the $3\pi \to \bar{N}N$ transition.

Fig.5 Two–loop diagrams contributing to the imaginary parts of the isoscalar electromagnetic and isovector axial nucleon form factors.

Fig.6 Spectral distribution of the isoscalar electric and magnetic nucleon form factors weighted with $1/t^2$ in the heavy nucleon limit. Shown are $\mathrm{Im}\, G_M^S(t)/t^2$ (upper line) and $\mathrm{Im}\, G_E^S(t)/t^2$ (lower line).

Fig.7 Spectral distribution of the isovector axial nucleon form factor weighted with $1/t^2$ in heavy nucleon limit.

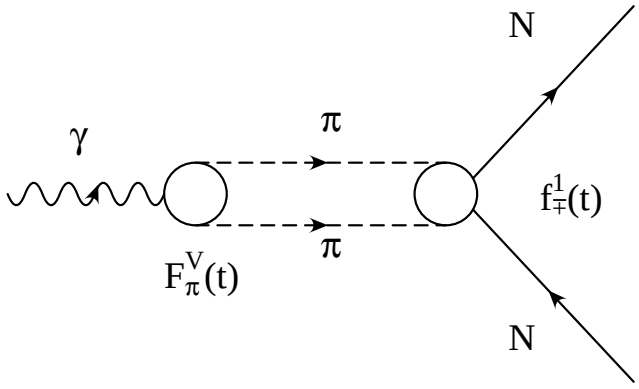


Figure 1

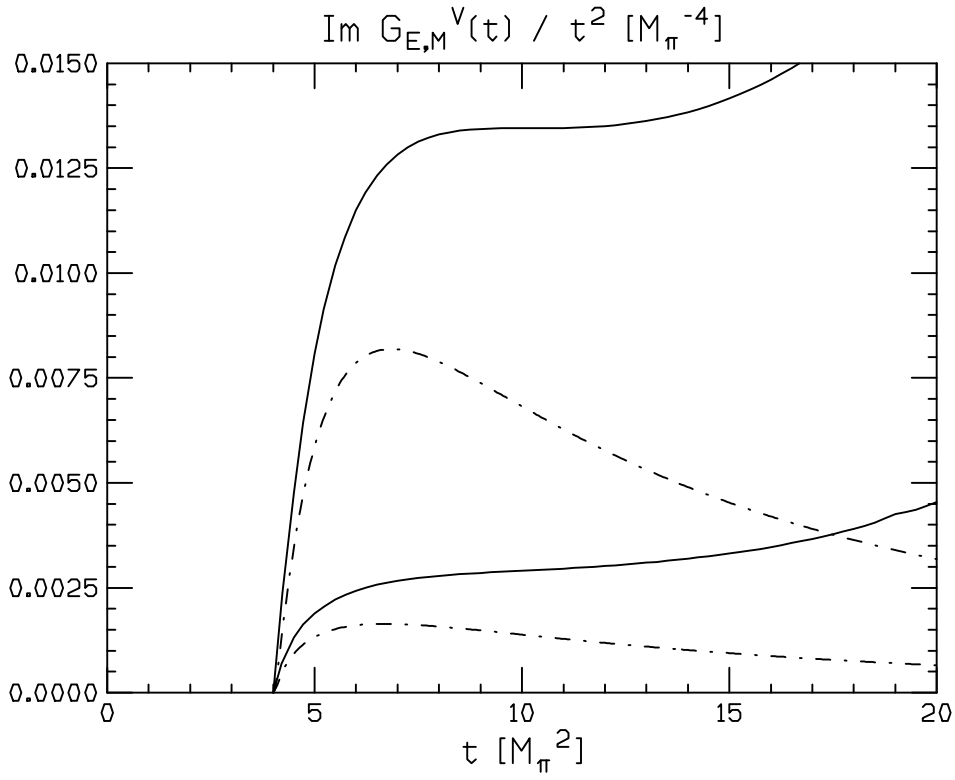


Figure 2

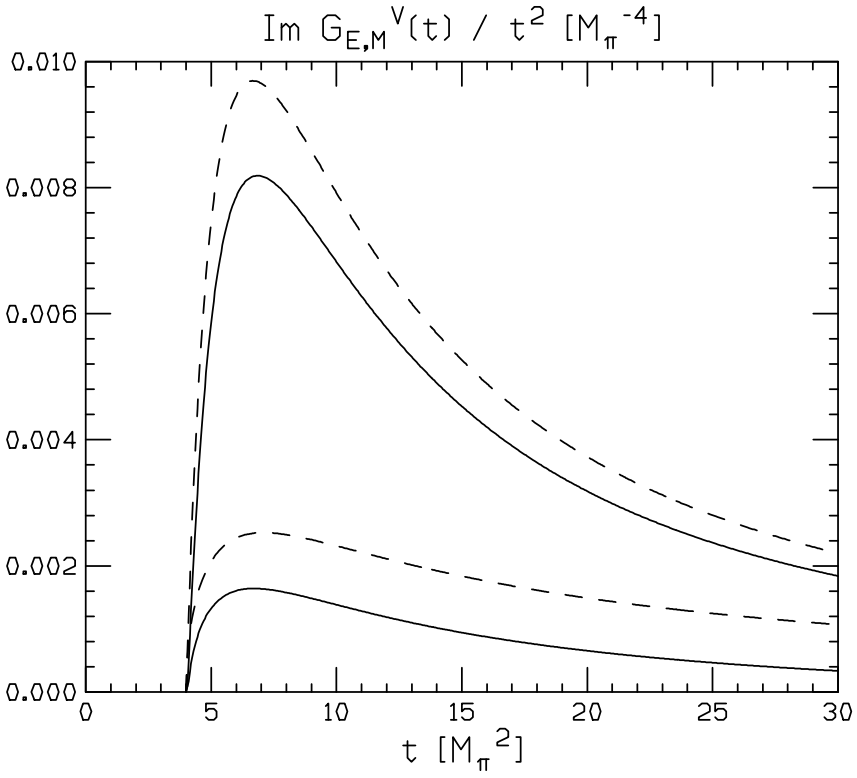


Figure 3

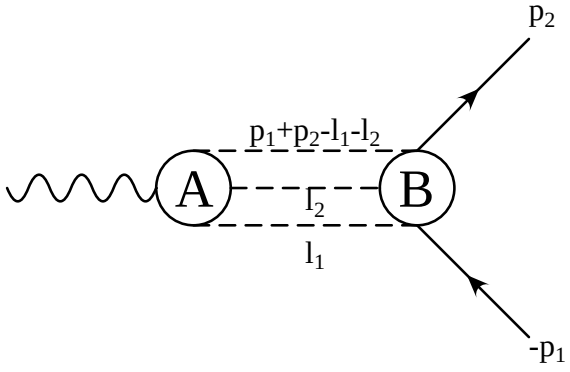


Figure 4

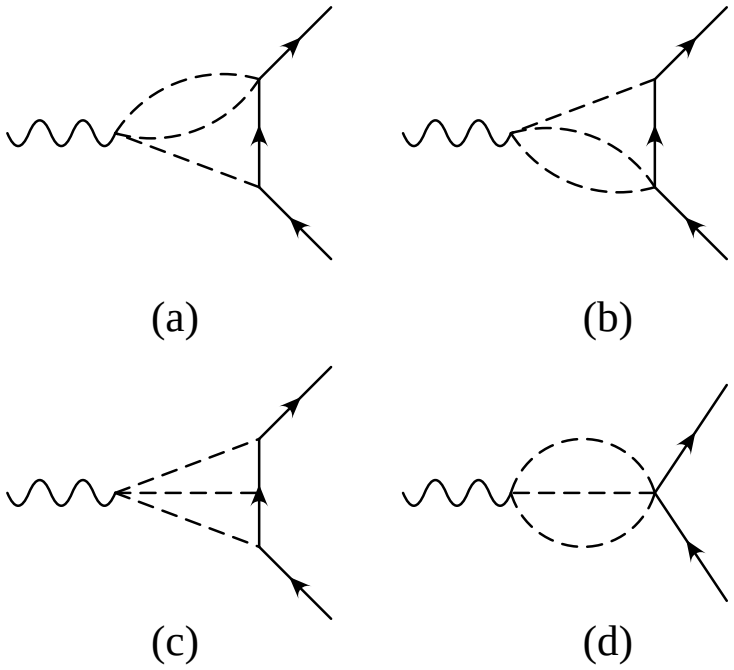


Figure 5

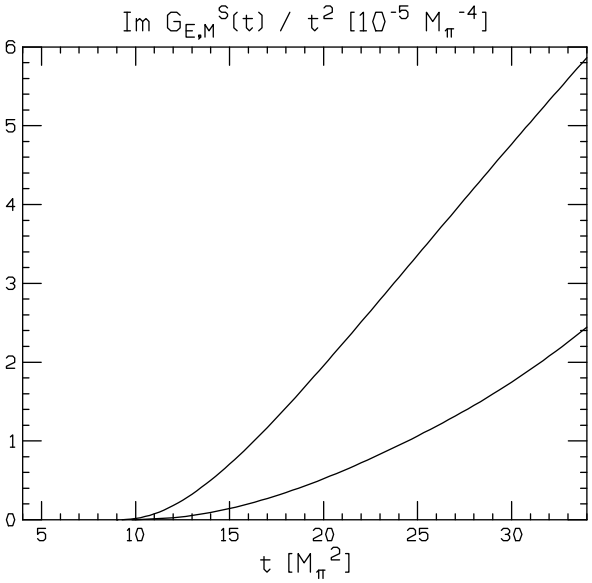


Figure 6

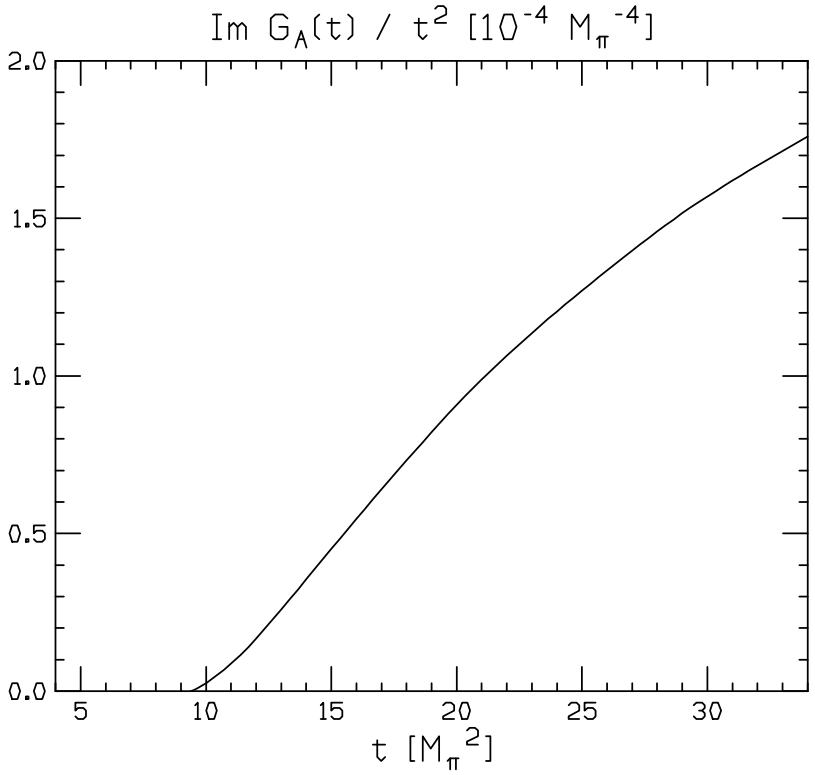


Figure 7